8.5 Terrain conductivity meters

A simple electromagnetic geophysical reconnaissance tool is the terrain conductivity meter (McNeill, 1980). This frequency-domain instrument operates as a purely inductive system in which transmitter (TX) and receiver (RX) loops do not make electrical contact with the ground. The two loops are magnetically flux-linked to each other and to the conductive ground as shown schematically by the circuits in Figure 8.7. Two popular terrain conductivity meters are the Geonics EM31 and EM34 instruments shown in Figure 8.9. The EM31 operates at 9.8 kHz and has TX–RX intercoil spacing of 3.66 m. The EM34 has three different intercoil spacings: 10, 20, and 40 m; these operate at, respectively, 6.4, 1.6 and 0.4 kHz. The EM34 can be used with vertical coplanar coils (horizontal dipole, or HD mode), as shown in the figure, or horizonal coplanar coils (vertical dipole, or VD mode) in which case the coils are laid flat on the ground.

The operating principle of the terrain conductivity meter is based on classical EM induction theory. A time-harmonic current of the form $I(t) = I\sin(\omega t)$ is passed through the TX loop. The primary magnetic field due to the current flowing in the transmitter loop is in-phase with the current and consequently has the form

$$\mathbf{B}^P(\rho, t) = \mathbf{B}_0(\rho)\sin(\omega t), \tag{8.17}$$

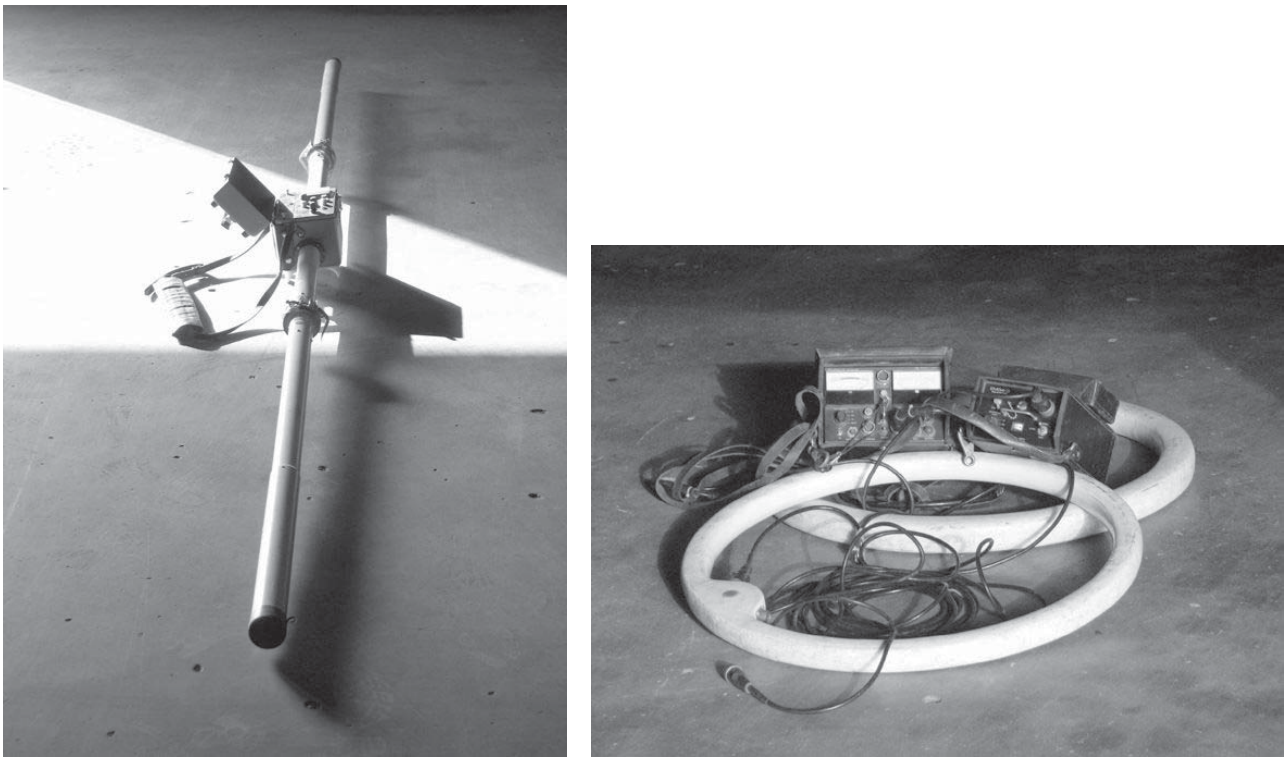

Figure 8.9 Terrain conductivity meters: (left) Geonics EM31; (right) Geonics EM34.

where ρ is the radial distance in a cylindrical coordinate system originated at the center of the TX loop. The conductive ground responds to the imposition of the time-varying primary magnetic flux by establishing a system of electromagnetic eddy currents whose secondary magnetic field $\mathbf{B}^S(\rho, t)$ is organized such that it tends to oppose the *change* $\partial\mathbf{B}^P/\partial t$ in primary flux. This principle was earlier captured in the circuit analogy by Equation (8.4). Essentially, the changing primary flux establishes an *electromotive force* (emf) in the ground. The ground then responds by generating a *back-emf* in an effort to restore the equilibrium that existed before the change occurred in the primary flux. This behavior accords with Lenz's law of electromagnetics, which (like homeostasis) is a specific case of Le Chatelier's principle in chemistry:

> If a system at equilibrium experiences a change of state, the equilibrium will shift in a direction so as to counter-act the imposed change.

The secondary magnetic field then has the form

$$\mathbf{B}^S(\rho, t) = \mathbf{B}_1(\rho)\sin(\omega t + \varphi). \tag{8.18}$$

where $|\mathbf{B}_1| << |\mathbf{B}_0|$, and φ is the phase shift caused by the induced currents which are not completely in-phase with the primary magnetic flux. The magnitude of the phase shift depends on the electrical conductivity of the ground. If the ground is perfectly conducting, $\varphi = 90^\circ$ and the secondary magnetic field is completely out of phase. If the ground is perfectly resistive, $\varphi = 0$ and the secondary magnetic field is completely in-phase. In general, the secondary magnetic field is *delayed* and *attenuated* with respect to the primary magnetic field, indicative of EM induction as an energy-dissipating d/dt process.

Using the identity

$$\sin(\omega t + \varphi) = \sin\omega t\cos\varphi + \cos\omega t\sin\varphi \tag{8.19}$$

we can decompose the total magnetic field $\mathbf{B}^T(\rho, t) = \mathbf{B}^P(\rho, t) + \mathbf{B}^S(\rho, t)$ into two orthogonal components:

$$\begin{aligned}\mathbf{B}^T(\rho, t) &= \mathbf{B}_0(\rho)\sin\omega t + \mathbf{B}_1(\rho)\sin(\omega t + \varphi)\\ &= \mathbf{B}_0(\rho)\sin\omega t + \mathbf{B}_1(\rho)\sin\omega t\cos\varphi + \mathbf{B}_1(\rho)\cos\omega t\sin\varphi\\ &= [\mathbf{B}_0 + \mathbf{B}_1\cos\varphi]\sin\omega t + [\mathbf{B}_1\sin\varphi]\cos\omega t\end{aligned} \tag{8.20}$$

such that $R = |\mathbf{B}_0 + \mathbf{B}_1\cos\varphi|$ is termed the *real* (*in-phase*) *response* and $Q = |\mathbf{B}_1\sin\varphi|$ is termed the *quadrature* (*out-of-phase*) *response*. The quantities (R, Q) are measured by the EM instrument. The quadrature signal is very small since in most cases,

$$\frac{|\mathbf{B}_1|}{|\mathbf{B}_0|} \sim 10^{-6} = 1\text{ppm}. \tag{8.21}$$

This implies that the strength of the induced current is only a very small fraction of the strength of the primary transmitted current, the latter being typically 1–3 A. The quadrature signal reveals information about the Earth since it vanishes ($Q = 0$) if the conductive Earth is not present. Notice that the known primary signal $\mathbf{B}_0$ can be subtracted to form a secondary in-phase response $R_S = |\mathbf{B}_1\cos\varphi|$. Instead of the real and quadrature

components, an EM system can also measure the *amplitude* and *phase* of the ground response. In terms of the quantities (R_S, Q), the amplitude is given by

$$A = \sqrt{R_S^2 + Q^2} = \sqrt{(\mathbf{B}_1 \cos\varphi)^2 + (\mathbf{B}_1 \sin\varphi)^2} = |\mathrm{B}_1|, \tag{8.22}$$

as required, while the phase is

$$\varphi = \tan^{-1}\frac{Q}{R_S} = \tan^{-1}\frac{\mathbf{B}_1 \sin\varphi}{\mathbf{B}_1 \cos\varphi} = \tan^{-1}(\tan\varphi) = \varphi \tag{8.23}$$

as required.

It is demonstrated below that the measured quadrature response Q can be interpreted in terms of the apparent ground conductivity σ_a. An *apparent conductivity* is defined as the conductivity of a homogeneous halfspace that would generate a quadrature response that is identical to the one that is observed. Keep in mind that $\sigma_a = \sigma_a(\omega)$ for an inhomogeneous geological formation since the signal penetration depth depends on frequency, according to the skin effect.

It can be shown that the normalized secondary vertical magnetic field ($b_z^{\mathrm{S}}/b_z^{\mathrm{P}}$) for coils operating in the VD mode over homogeneous ground, assuming a small horizontal TX loop such that loop radius $a/\rho << 1$, can be simplified to (Wait, 1954; McNeill, 1980):

$$\left(\frac{b_z^S}{b_z^P}\right)_V \approx -\frac{2}{\alpha^2\rho^2}\{9 - [9 - 9i\alpha\rho - 4\alpha^2\rho^2 + i\alpha^3\rho^3]\exp(i\alpha\rho)\}, \tag{8.24}$$

where $\alpha^2 = -i\mu_0\sigma\omega$. Furthermore, at low induction numbers,

$$\mathrm{B} \equiv \frac{\rho}{\delta} \ll 1, \text{ orequivalently, } |\alpha\rho| \ll 1, \tag{8.25}$$

such that the TX–RX separation distance is much less than the electromagnetic skin depth (equivalent also to low frequency), it is straightforward to show that Equation (8.24) reduces to

$$\left(\frac{b_z^S}{b_z^P}\right)_V \approx 1 - \frac{i\mu_0\omega\sigma\rho^2}{4}. \tag{8.26}$$

The VD-mode apparent conductivity σ_a is then obtained by re-arranging the out-of-phase component of Equation (8.26),

$$\sigma_a = \frac{4}{\mu_0\omega\rho^2}\left|\mathrm{Im}\left(\frac{b_z^S}{b_z^P}\right)\right|. \tag{8.27}$$

Similarly, when the TX and RX coils are oriented in the HD mode, the normalized secondary field is approximated by (McNeill, 1980)

$$\left(\frac{b_z^S}{b_z^P}\right)_H = 2\left\{1 + \frac{3}{\alpha^2\rho^2} - [3 - 3i\alpha\rho - \alpha^2\rho^2]\frac{\exp(i\alpha\rho)}{\alpha^2\rho^2}\right\}, \tag{8.28}$$

and an equation identical in form to Equation (8.27) holds for the HD-mode apparent conductivity.

To summarize, the terrain conductivity meter, e.g. Geonics EM31 or EM34, reads an apparent conductivity that is linearly related to the measured quadrature response by $\sigma_a = 4Q_N/\mu_0\omega\rho^2$ where $Q_N = |\mathrm{Im}(b_z^S/b_z^P)_V|$ or $Q_N = |\mathrm{Im}(b_z^S/b_z^P)_H|$ depending on whether the instrument is being used in the VD or the HD mode.

The above discussion describes the basic operating principle of low-induction-number (LIN) terrain conductivity meters. The meter will fail, or exhibit erratic behavior including displaying negative apparent conductivities, in resistive terrain if the conductivity is sufficiently low such that the quadrature response Q_N falls below the system noise level. Resistive geological materials cannot sustain strong systems of induced currents. The terrain conductivity meter generates stable readings in conductive terrains, for example, $\sigma \sim 0.001$–0.1 S/m, since in these cases the quadrature response is large compared to the system noise level. The meter may also report negative apparent conductivities in the vicinity of strong lateral heterogeneities, such as might be caused by pipelines or faults, as the assumption of a homogeneous ground that was used to derive Equation (8.24) is not applicable in these cases. Finally, in highly conductive terrains the low-induction number (LIN) assumption (8.25) breaks down and the apparent conductivity σ_a no longer scales linearly with the measured quadrature response Q_N. In such cases, a correction factor such as the one proposed by Beamish (2011) should be applied to better estimate the apparent conductivity.

Measurements using a LIN terrain conductivity meter were taken by geophysics undergraduate students over a buried natural-gas pipeline on Riverside campus at Texas A&M University. The results are shown in Figure 8.10. Data were taken along a profile crossing the pipeline, with a Geonics EM31 instrument resting on the ground. Two orientations of the EM31 instrument were used: the in-line (left), or *P-mode*, in which the TX and RX coils are aligned with the profile direction; and the broadside (right), or *T-mode*, in which the TX and RX coils are aligned perpendicular to the profile direction (i.e. parallel to the pipeline). It is easy to see that the pipeline generates a strong, repeatable EM31 anomaly with high signal-to-noise ratio, for both modes. Notice there are some unphysical negative apparent conductivities in the P-mode profile in the vicinity of the pipepline. The striking differences between the P-mode and T-mode signatures reflect the variation in mutual electromagnetic coupling between the TX coil, the subsurface target, and the RX coil caused by differences in the relative geometry of the two modes relative to the target. At the beginning and the end of the profiles, both sets of EM31 readings tend to values of ~ 60–70 mS/m, regardless of the orientation of the coils, reflecting the relatively homogeneous background soil conditions.

A more comprehensive analysis of the EM31 response to a highly conductive target was performed by Benavides and Everett (2005). In that study, which has applications to EM imaging in areas with high cultural noise, a number of steel drill pipes were laid out on the ground in the pattern shown in Figure 8.11a. The P-mode and T-mode responses are shown in Figure 8.11b and 8.11c, respectively. The line spacing is 1.0 m and station spacing is 0.25 m. The data were acquired along north–south profiles. It is evident that the pipes generate elongate, bimodal anomalies that are oriented in the direction of the TX–RX coils. The smallest target, the drill pipe collar (item 4), generates only a subtle anomaly in each mode. The anomalies are highlighted if the difference between the T-mode and the P-mode

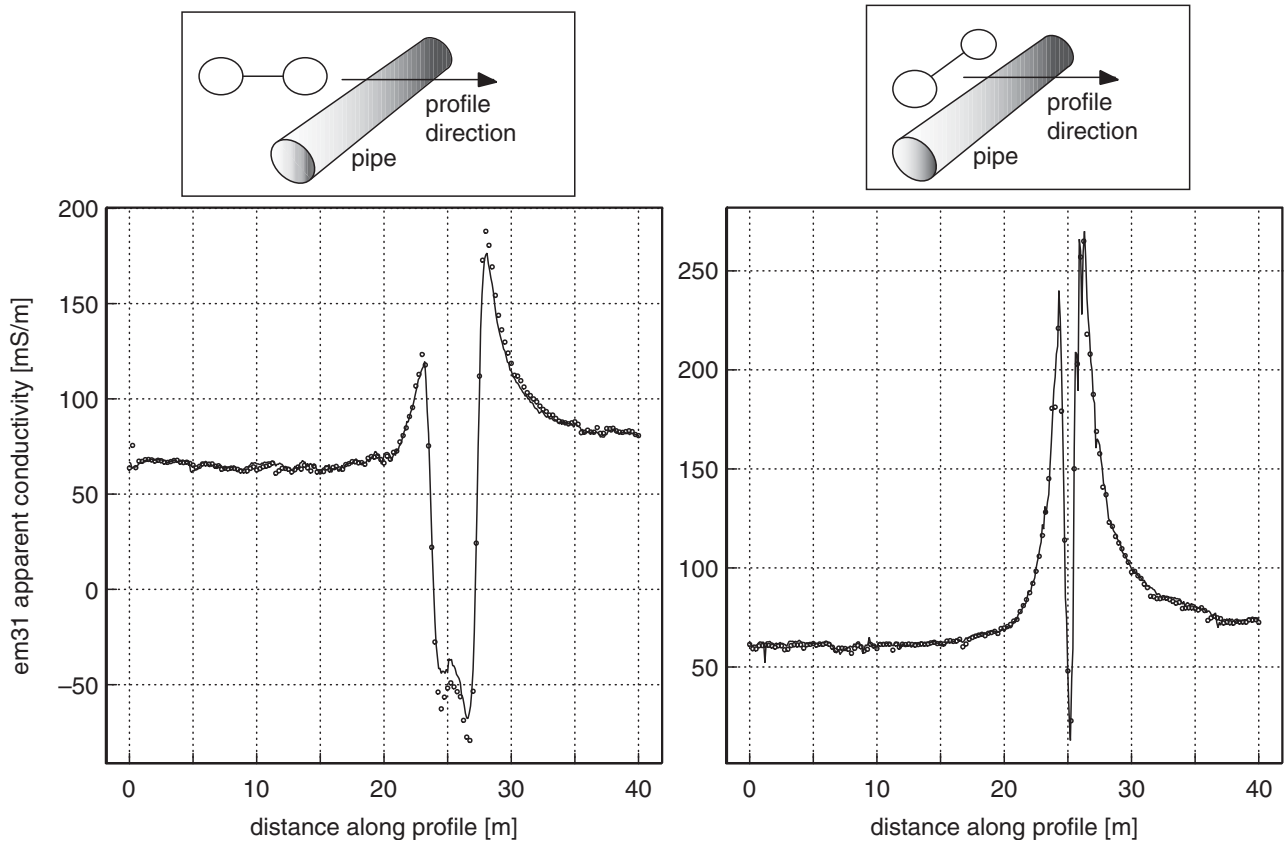

Figure 8.10 EM31 in-line P-mode (left side) and broadside T-mode (right side) signatures of the natural-gas pipeline at Texas A&M Riverside campus. Solid lines indicate original survey with 0.1-m station spacing. Symbols indicate repeat survey with 0.25-m station spacing.

signatures is plotted, as shown in Figure 8.10d. In this presentation, the pipe anomalies exhibit a distinctive quadrupole morphology, while the background soil response remains very subdued. Notice, however, that it is not easy to see from the geophysical signature that the drill pipe (item 5) is aligned at ~ 45° to the data-acquisition grid.

Terrain conductivity meters can also be used for mapping lateral contrasts in near-surface geology. Figure 8.12, left, illustrates EM34 readings taken with 10-m TX–RX intercoil spacing in the P-mode with the coil axes vertical (VD). The profile crosses a known lateral discontinuity juxtaposing a gravel unit with a sand/clay interbedded unit. The purpose of the survey was to delineate the extent of a paleochannel comprised of coarse sediment, in this case, an economic gravel deposit. Generally speaking, fine-grained material with abundant clay is more conductive than clean, coarse-grained sediment. The abrupt transition from low to high apparent conductivity marks the lateral boundary of the gravel paleochannel.

In Figure 8.12, right, the EM34 method (P-mode, VD) is used in its three different TX–RX intercoil spacings (10, 20, and 40 m) to map faults and stratigraphic contacts in a well-characterized consolidated sandstone aquifer in central Texas. The Hickory sandstone, of Cambrian age, is divided into lower, middle, and upper units. It is known that the faults and contacts act as barriers and conduits compartmentalizing groundwater flow in this aquifer.

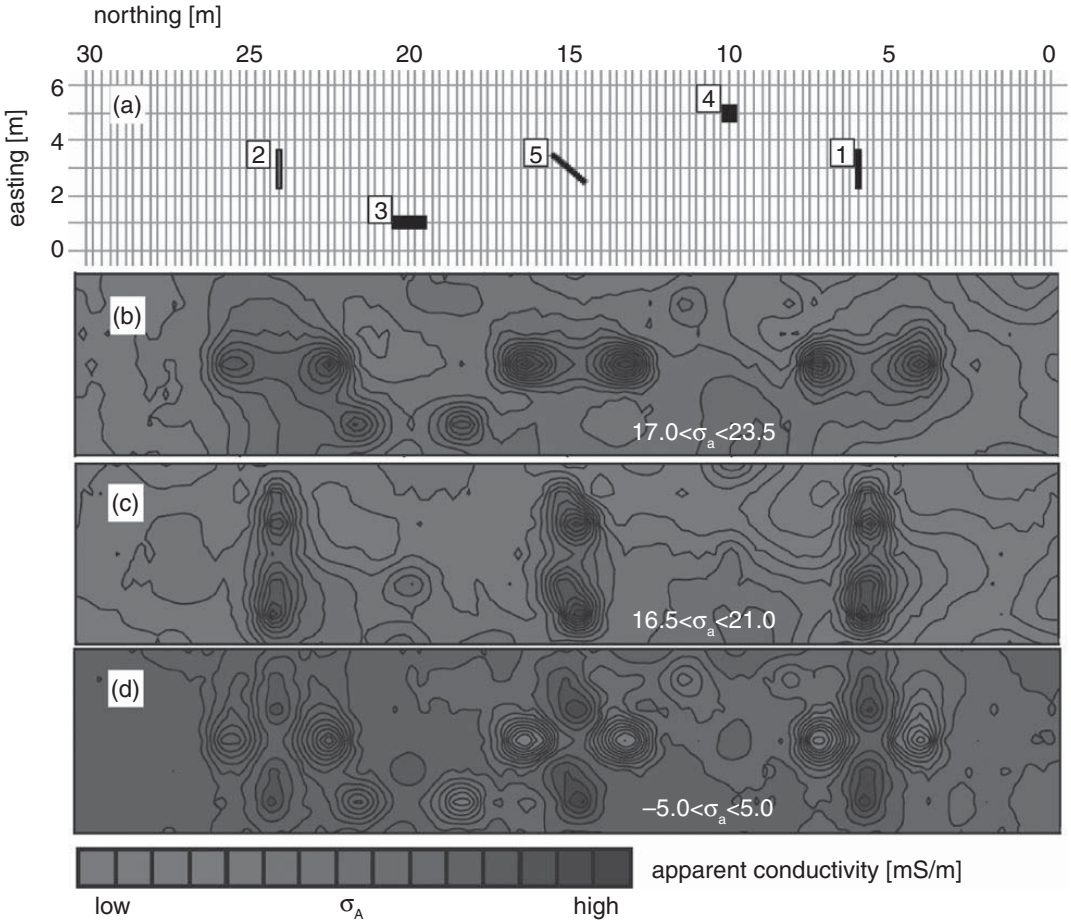

Figure 8.11 EM31 detection of conductive targets. (a) Experimental layout of steel pipes; (b) P-mode apparent conductivity map; (c) T-mode apparent conductivity map; (d) difference of the T-mode and P-mode maps; key: 1, 5 = 155 × 12.4-cm drill pipe, 2 = 150 × 6.4-cm drill pipe, 3 = 75 × 7.5-cm galvanized iron water pipe, 4 = 28 × 7.2-cm drill pipe collar. After Benavides and Everett (2005).

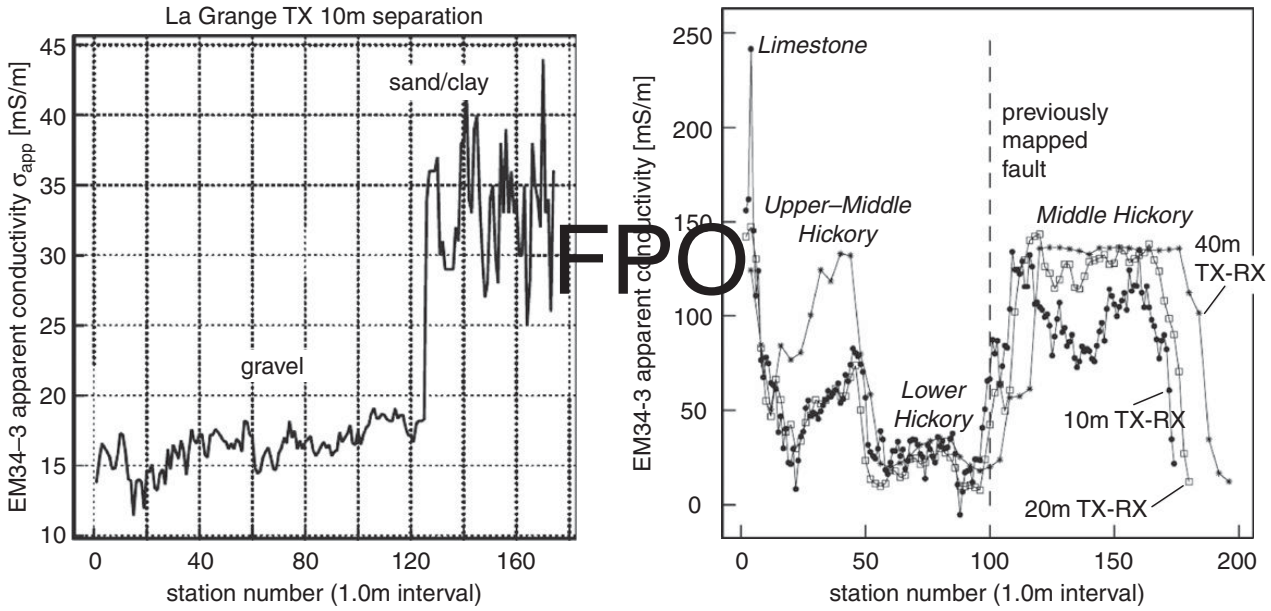

Figure 8.12 EM34 mapping of lateral geological discontinuities: (left) gravel quarry; (right) faulted Cambrian sandstone aquifer. After Everett and Meju (2005).

The observed lateral contrasts in apparent electrical conductivity are caused by lateral variations in sedimentary texture. For example, the location of a previously mapped, buried fault is shown by the dotted line. The variations in the EM34 responses between stations 20–50 can be explained in terms of spatial variations in the distribution of clays within the Hickory sandstone formation (Gorman *et al*., 1998).

8.6 Time-domain EM induction

A physical understanding of *transient* CSEM responses can be obtained by recognizing that the induction process is equivalent to the diffusion of an image of the transmitter (TX) loop into a conducting medium. The similarity of the equations governing electromagnetic induction and hydrodynamic vortex motion, first noticed by Helmholtz, leads directly to the association of the image current with a smoke ring (Lamb, 1945; p. 210). The latter is not "blown," as commonly thought, but instead moves by self-induction with a velocity that is generated by the smoke ring's own vorticity and described by the familiar Biot–Savart law (Arms and Hama, 1965). An electromagnetic smoke ring dissipates in a conducting medium much as the strength of a hydrodynamic eddy is attenuated by the viscosity of its host fluid (Taylor, 1958; pp. 96–101). The material property that dissipates the electromagnetic smoke ring is electrical conductivity.

The operating principles of an inductively coupled time-domain electromagnetic (TDEM) system are summarized as follows. A typical current waveform $I(t)$ consists of a slow rise to a steady value of I_0 followed by a rapid shut-off as exemplified by the linear ramp shown in Figure 8.13a. Passing such a disturbance through the TX loop generates a primary magnetic field that is in-phase with, and proportional to, the TX current. According to Faraday's law of induction, an impulsive electromotive force (emf) that scales with the negative time rate of change of the primary magnetic field is also generated. The emf drives electromagnetic eddy currents in the conductive Earth, notably in this case during the ramp-off interval, as shown in Figure 8.13b. After the ramp is terminated, the emf vanishes and the eddy currents start to decay via Ohmic dissipation of heat. A weak, secondary magnetic field is produced in proportion to the waning strength of the eddy currents. The receiver (RX) coil voltage measures the time rate of change of the decaying secondary magnetic field, Figure 8.13c. In many TDEM systems, RX voltage measurements are made during the TX off-time when the primary field is absent. The advantage of making off-time measurements is that the relatively weak secondary signal is not swamped by the much stronger primary signal. A good tutorial article on TDEM has been written by Nabighian and Macnae (1991).

During the ramp-off, the induced current assumes the shape of the horizontal projection, or shadow, of the TX loop onto the surface of the conducting ground. The sense of the circulating induced currents is such that the secondary magnetic field they create tends to maintain the total magnetic field at its original steady-on value prior to the TX ramp-off. In this case, therefore, the induced currents flow in the same direction as the TX current, i.e. opposing the TX current decrease that served as the emf source. The image current then

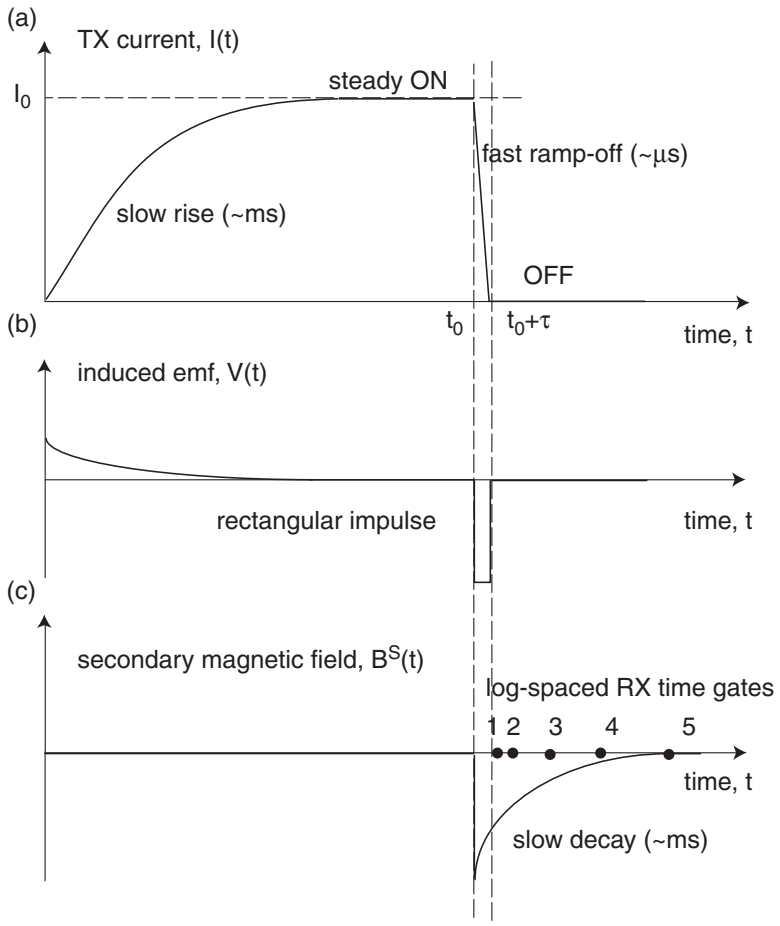

Figure 8.13 (a) A typical TX waveform $I(t)$ with slow rise and fast ramp-off; (b) induced emf $V(t)$ proportional to the time rate of change of the primary magnetic field; (c) the decaying secondary magnetic field $B^S(t)$ due to dissipation of currents induced in the ground.

diffuses downward and outward while diminishing in amplitude. A series of snapshots in Figure 8.14 of the secondary electric field intensity illustrates the transient diffusion of the electromagnetic smoke ring into a uniform halfspace.

In the widely used central-loop sounding method, the RX loop is placed at the center of the TX loop, while in TDEM offset-loop soundings the TX and RX loops are separated by some distance L. As indicated in Figure 8.15, at a fixed instant in time t, the vertical magnetic field $H_z(L)$ due to the underground smoke ring exhibits a sign change from positive to negative as distance L increases. In other words, the vertical magnetic field $H_z(t)$ changes sign from positive to negative as the smoke ring passes beneath a fixed measurement location. It should be clear to the reader that a central-loop measurement of the vertical magnetic field $H_z(t)$ does not exhibit such a sign change.

The "normal moveout" of the sign reversal with increasing TX–RX separation distance L is shown in Figure 8.16. The sharp cusps in the response curves mark the transition between positive and negative flux passing through a RX loop placed at distance L from the TX loop. These solutions correspond to the response of a uniform halfspace of $\sigma \sim 0.1$ S/m, as indicated in the figure legends. Note the late-time responses scale as a power law of

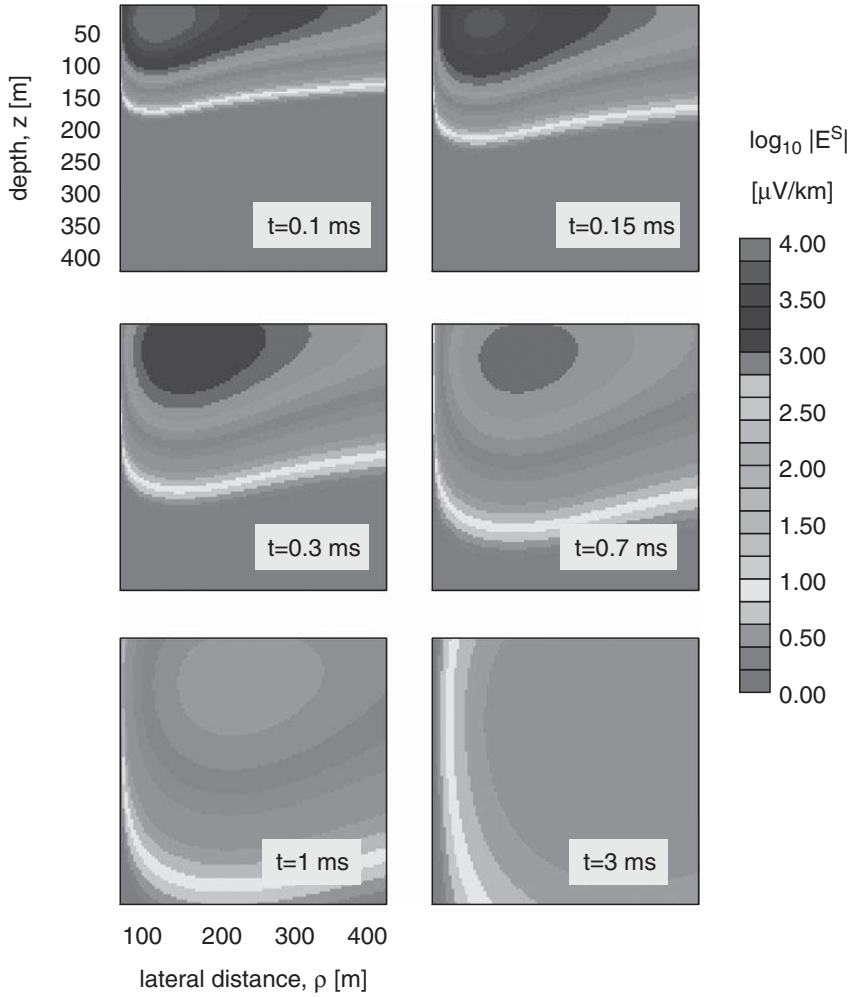

Figure 8.14 Transient smoke-ring diffusion into a uniformly conductive halfspace, $\sigma = 0.1$ S/m.

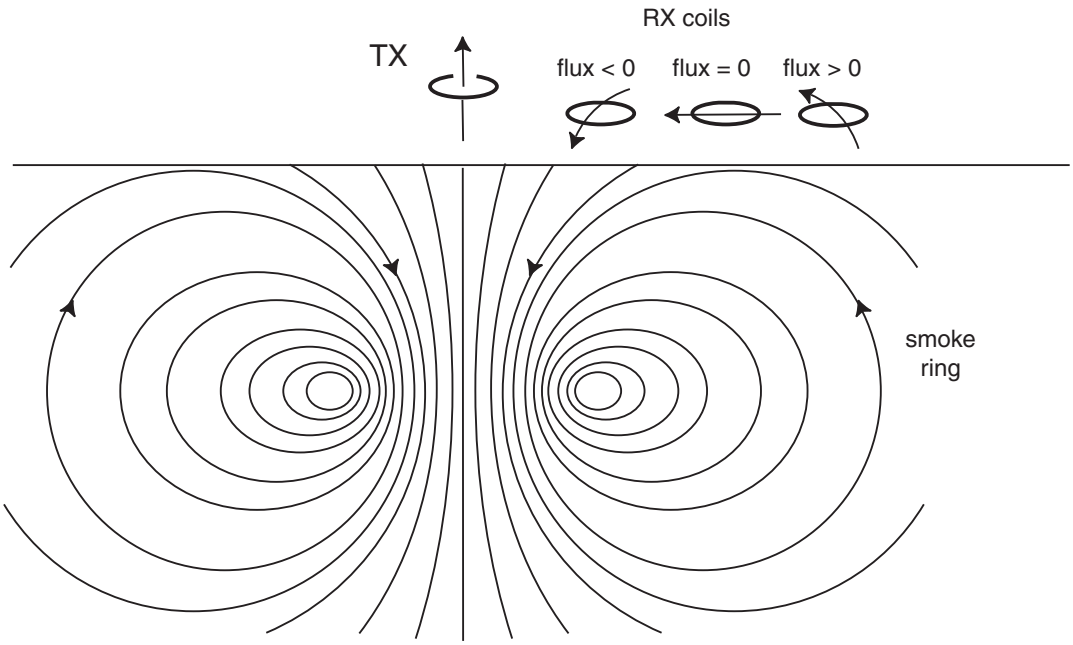

Figure 8.15 The changing sign of magnetic flux from the smoke ring as a function of TX–RX separation. After Nabighian and Macnae (1991).

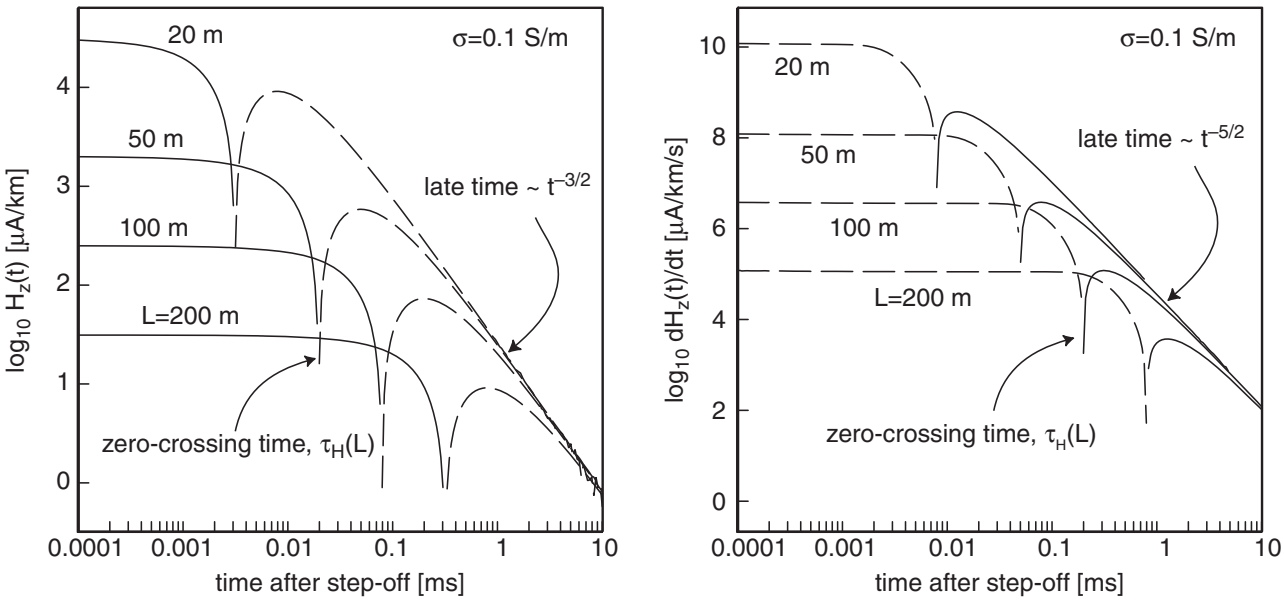

Figure 8.16 (Left) Transient step-off vertical magnetic-field response, horizontal loop source; (right) transient step-off RX voltage response, horizontal loop source.

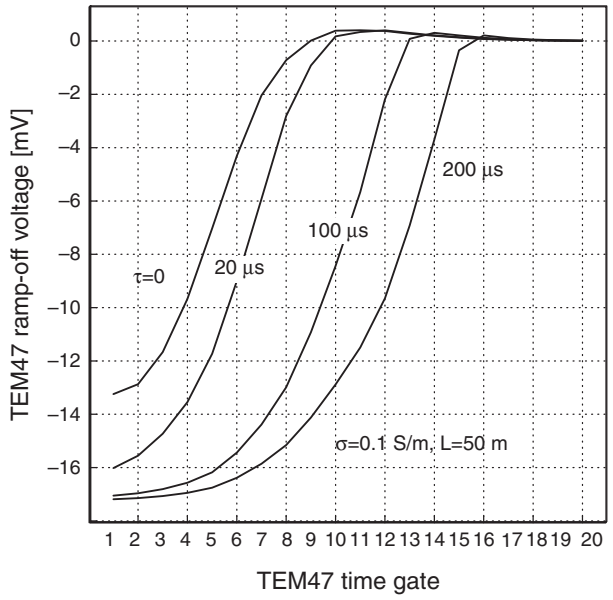

Figure 8.17 Effect of finite ramp-off time on TEM47 response.

the form $t^{-3/2}$ for the magnetic field and, since it is proportional to the time-derivative of the magnetic field, of the form $t^{-5/2}$ for the induction-coil response.

In the ideal TDEM case, step-off transients are analyzed. However, it is impractial in the field to abruptly switch off the current in a finite-sized loop due to self-inductance effects. Consequently, most systems are linearly ramped off over a brief time interval on the order of microseconds. The impact of using a finite TX ramp-off time on the TDEM response is shown in Figure 8.17. For fixed TX–RX separation L, an increase in the ramp-off time τ

serves to delay the response measured at the receiver. The curves in Figure 8.17 are simulated Geonics TEM47 (a popular commercial TDEM instrument) responses that have been computed by convolving the theoretical impulse reponse with a linear ramp-off function of width τ (Fitterman and Anderson, 1987). The curve labeled $\tau = 0$ is the ideal step-off response. The curves are plotted for the logarithmically-spaced times, after initiation of the ramp-off, at which the TEM47 system samples the response.

8.7 Finite-source excitation of a layered Earth

A classic problem of considerable practical importance in near-surface applied geophysics is to determine the electromagnetic response of a plane-layered Earth to finite-source excitation. There are well-known analytic solutions to the Maxwell equations available for finite-sized loops of horizontal and vertical orientation and horizontal grounded sources of finite length; while these are broadly scattered throughout the literature, many are derived in Ward and Hohmann (1989).

In this section we indicate some analytic frequency-domain solutions to a few problems of inductive or grounded-source sounding of a layered halfspace. For example, the electromagnetic response of a horizontal loop source of finite radius, like that shown in Figure 8.18, is derived in Morrison *et al*. (1969) and Ryu *et al*. (1970).

From the complete derivation given in Appendix D, the vertical magnetic field recorded by an RX coil placed on the surface $z = 0$ above a homogeneous ground is found to be

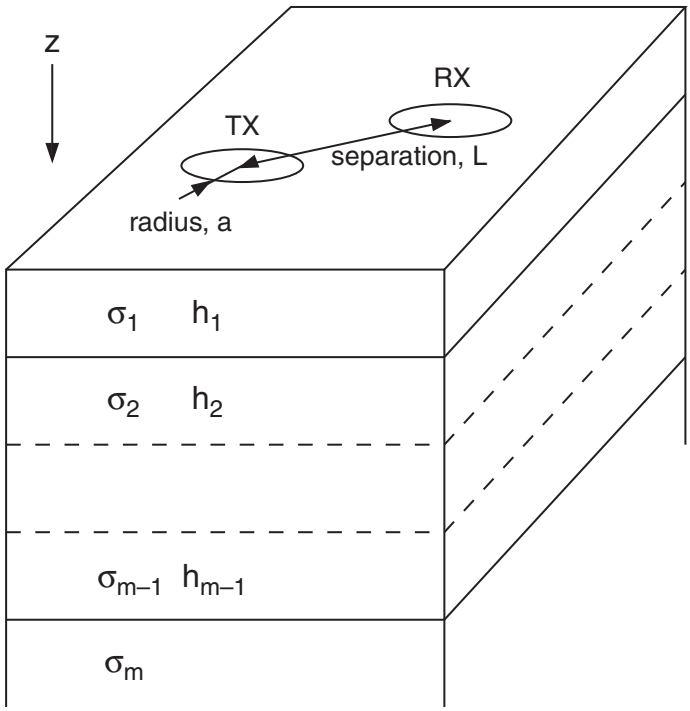

Figure 8.18 Horizontal TX and RX loops on a layered halfspace.